Electronic Supplementary Information (ESI)

Enhancing Electrostatic Interactions to Activate Polar Molecules: Ammonia Borane Methanolysis on Cu/Co(OH)$_2$ Nanohybrid

Qian-Qian Chen,[†ac] Qiang Li,[†b] Chun-Chao Hou,[a] Chuan-Jun Wang,[a] Cheng-Yun Peng,[a] Núria López[*b] and Yong Chen[*ac]

[a]Key Laboratory of Photochemical Conversion and Optoelectronic Materials & HKU-CAS Joint Laboratory on New Materials, Technical Institute of Physics and Chemistry, Chinese Academy of Sciences, Beijing 100190, P. R. China

[b]Institute of Chemical Research of Catolonia, ICIQ. The Barcelona Institute of Science and Technology, Ad. Països Catalans, 16, 43007, Tarragona, Spain

[c]University of Chinese Academy of Sciences, Beijing 100049, P. R. China

[*]E-mail：chenyong@mail.ipc.ac.cn and nlopez@iciq.es

[†]Qian-Qian Chen and Qiang Li contributed equally.

Theoretical Methods

For the $Co(OH)_2$ support, both the antiferromagnetic (AFM) and ferromagnetic (FM) bulk structures were optimized with GGA-PBE functional. Co has high spin states in both structures and AFM is slightly more stable than FM by 0.04 eV/cell. Then all the following calculations are based on the AFM structures. The Heyd-Scuseria-Ernzerhof hybrid functional (HSE06)[1] was employed to obtain the band gap of $Co(OH)_2$. The fraction of exact exchange in a Hartree-Fock/DFT hybrid functional type calculation was 15%, as HSE06 method overcorrects the DFT-inherent self-interaction error and leads to exceedingly large band gaps.[2,3] Calculated lattice parameters HSE06-15 are 6.384 and 4.701 Å for *a* and *c*, respectively, which agrees well with previous reported *a* and *c* values of 6.372 and 4.653 Å.[4] Then, U_{eff} of 4.00 eV was determined via comparing the band gap (2.28 eV) with different U values (Table S1) to the HSE06 result (2.22 eV).

Table S1. Band Gap and lattice parameters for DFT+U and HSE06 methods.

		Lattice Parameters		
U^{eff}/ eV	E gap/eV	a/Å	b/Å	c/Å
3.00	1.94	6.45	6.45	4.66
3.50	2.13	6.45	6.45	4.67
4.00	2.28	6.44	6.44	4.67
4.50	2.41	6.44	6.44	4.67
5.00	2.53	6.43	6.43	4.67
HSE-06	3.53	6.41	6.41	4.63
HSE-06-15	2.22	6.38	6.38	4.70
Exp.	/	6.37	6.37	4.65

Table S2. Bader charges ($|e^-|$) and *d*-band center (eV) with respect to the Fermi energy for Cu in Cu(111), and Co-Cu heterostructures. ^{u} and ^{d} stand for the upper and lower layers in the Co^2-Cu^2 structure.

	Bader Charges	*d*-band center
$Co\text{-}Cu^1$	0.28	-2.00
$Co\text{-}Cu^2$	0.14	-2.37
$Co\text{-}Cu^3$	0.10	-2.33
Cu(111)	0.00	-2.15
Co^2-Cu^2	0.26^u, 0.28^d	1.92^u, 2.00^d

For adsorbates on the surface, their adsorption energies are defined as:

$$Eads = E(slab+species) - E(slab) - E^{gas}(species) \qquad \text{Eq. S1}$$

With E(slab+species), E(slab), E^{gas} (species) are energies of species on surface, pure surface, and species in gas phase, respectively. Calculated adsorption energies are listed in Table S3.

The solvation energy of AB in methanol is -0.62 eV obtained via the MGCM method.[5]

Table S3. Adsorption energies $E_{ads}(X)$ of X = AB and methanol, activation barriers E_a, and reaction energies ΔE of the SN2 step on various surfaces. All values in eV.

	$E_{ads}(BH_3NH_3)$	E_{ads} (CH_3OH)	E_a(SN2)	ΔE(SN2)
$Co(OH)_2$	-0.42	-0.10	/	/
Co-Cu[1]	-0.92	-0.65	0.76	-1.10
Co-Cu[2]	-0.70	-0.56	0.89	-0.45
Co-Cu[3]	-0.76	-0.42	0.95	-0.50
Co^2-Cu^2	-1.13	-0.79	0.83	-0.29
Cu(111)	-0.54	-0.22	1.02	-0.47

Core-level shifts calculations have been performed to compare the XPS shift in Figure 2d in the manuscript. The Core-level shift energy, E_{CLS}, is defined as below:

$$E_{CLS} = \left[E^{n_c-1}_{Co-Cu^3} - E^{n_c}_{Co-Cu^3}\right] - \left[E^{n_c-1}_{Cu(111)} - E^{n_c}_{Cu(111)}\right] \qquad \text{Eq. S2}$$

With $E^{n_c-1}_{Co-Cu^3}$ and $E^{n_c-1}_{Cu(111)}$ are the energies of Co-Cu[3] and Cu(111) by removing one core electron of the surface atoms and adding it to the valance band. $E^{n_c}_{Co-Cu^3}$ and $E^{n_c}_{Cu(111)}$ are standard calculated energies of Co-Cu[3] and Cu(111) slab models. As the atoms in the first layer of Co-Cu[3] are not planar as those on Cu(111), $E^{n_c-1}_{Co-Cu^3}$ for all 25 atoms in the first layer have been calculated and the average energy is used in the above equation.

Table S4. Bader charges (in $|e^-|$) of B and N atoms in the initial (IS) and transition (TS) states on four model surfaces.

Surfaces	IS		TS	
	B	N	B	N
Cu111	1.70	-1.42	1.65	-1.20
Co-Cu^1	1.72	-1.35	1.69	-1.17
Co-Cu^2	1.75	-1.32	1.65	-1.20
Co-Cu^3	1.67	-1.40	1.68	-1.20
Co^2-Cu^2	1.70	-1.36	1.69	-1.10
Average	1.71	-1.37	1.67	-1.17

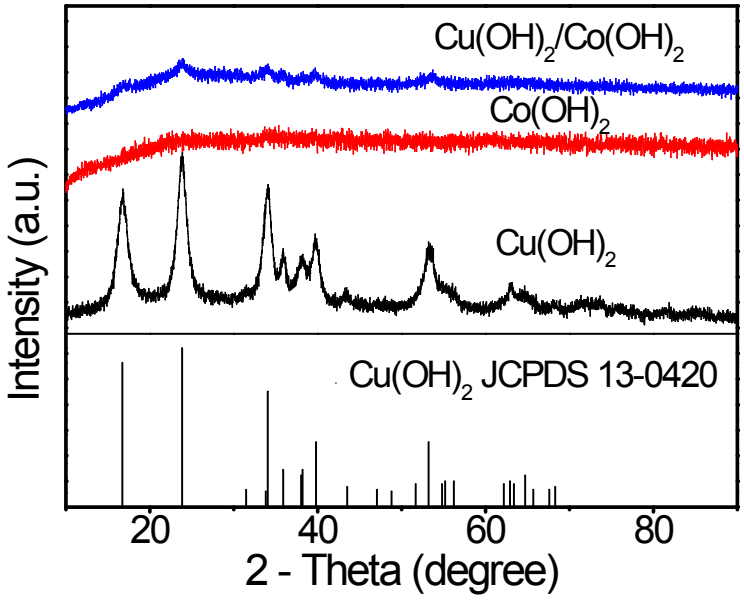

Fig. S1. XRD patterns of $Cu(OH)_2/Co(OH)_2$, $Co(OH)_2$ and $Cu(OH)_2$.

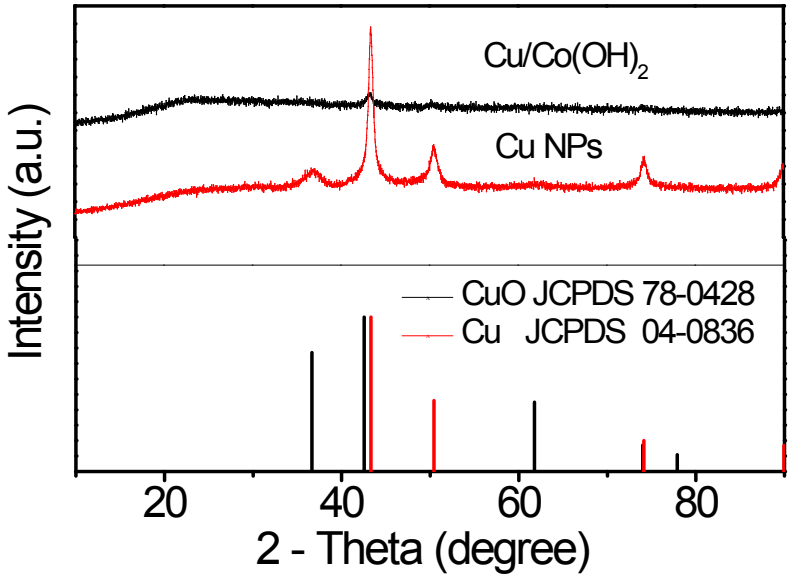

Fig. S2. XRD patterns of $Cu/Co(OH)_2$ and Cu NPs.

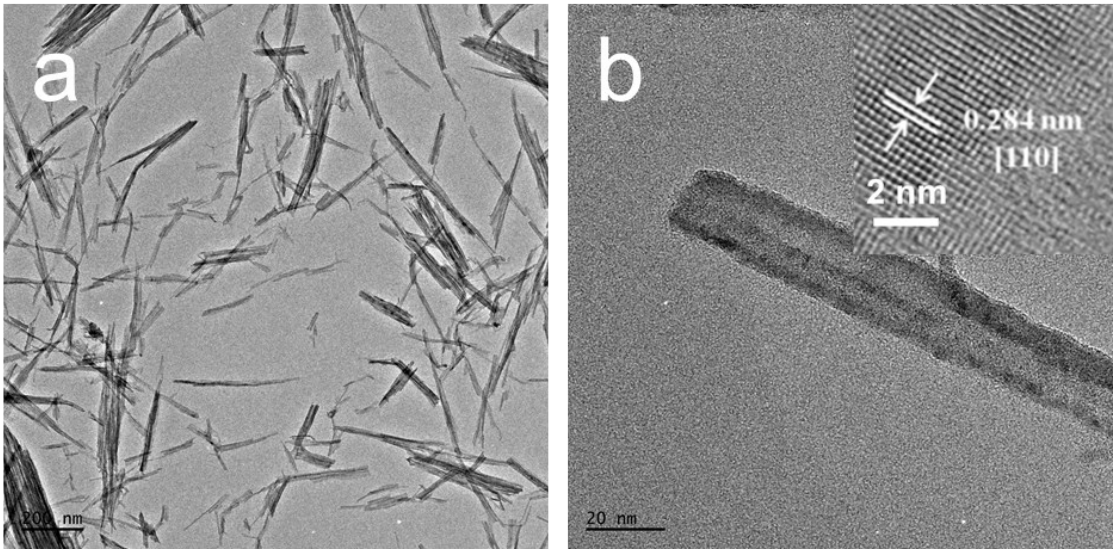

Fig. S3. (a) TEM image and (b) magnified TEM of $Cu(OH)_2$. Inset b: HRTEM of $Cu(OH)_2$.

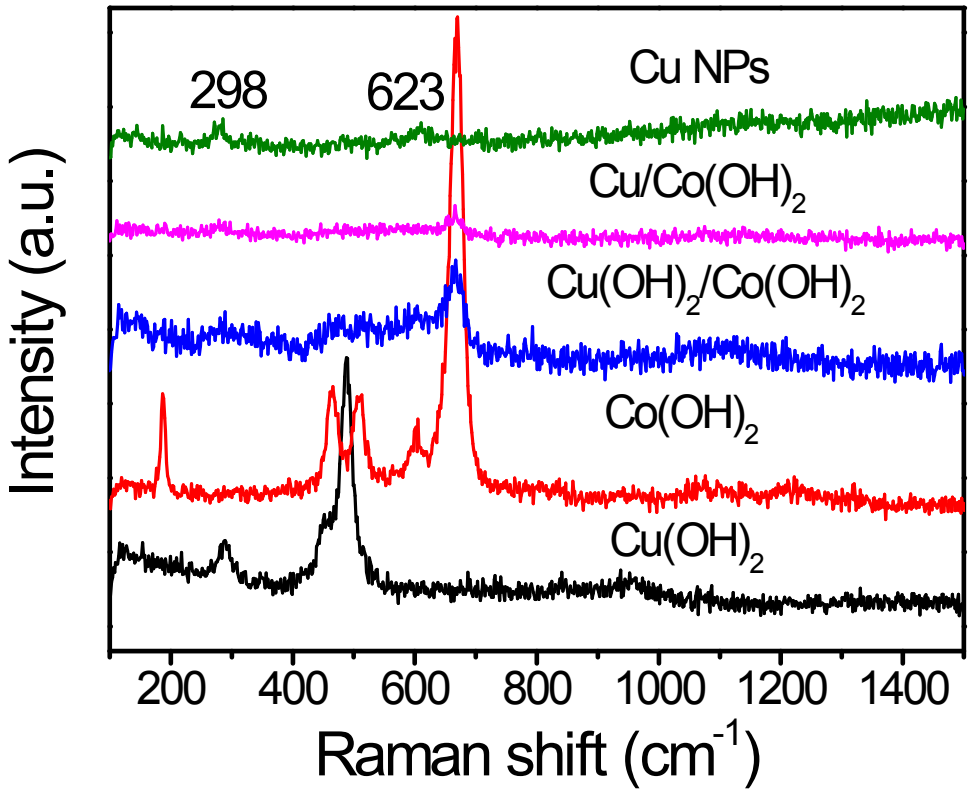

Fig. S4. Raman spectra of $Cu(OH)_2$, $Co(OH)_2$, $Cu(OH)_2/Co(OH)_2$, $Cu/Co(OH)_2$ and Cu NPs.

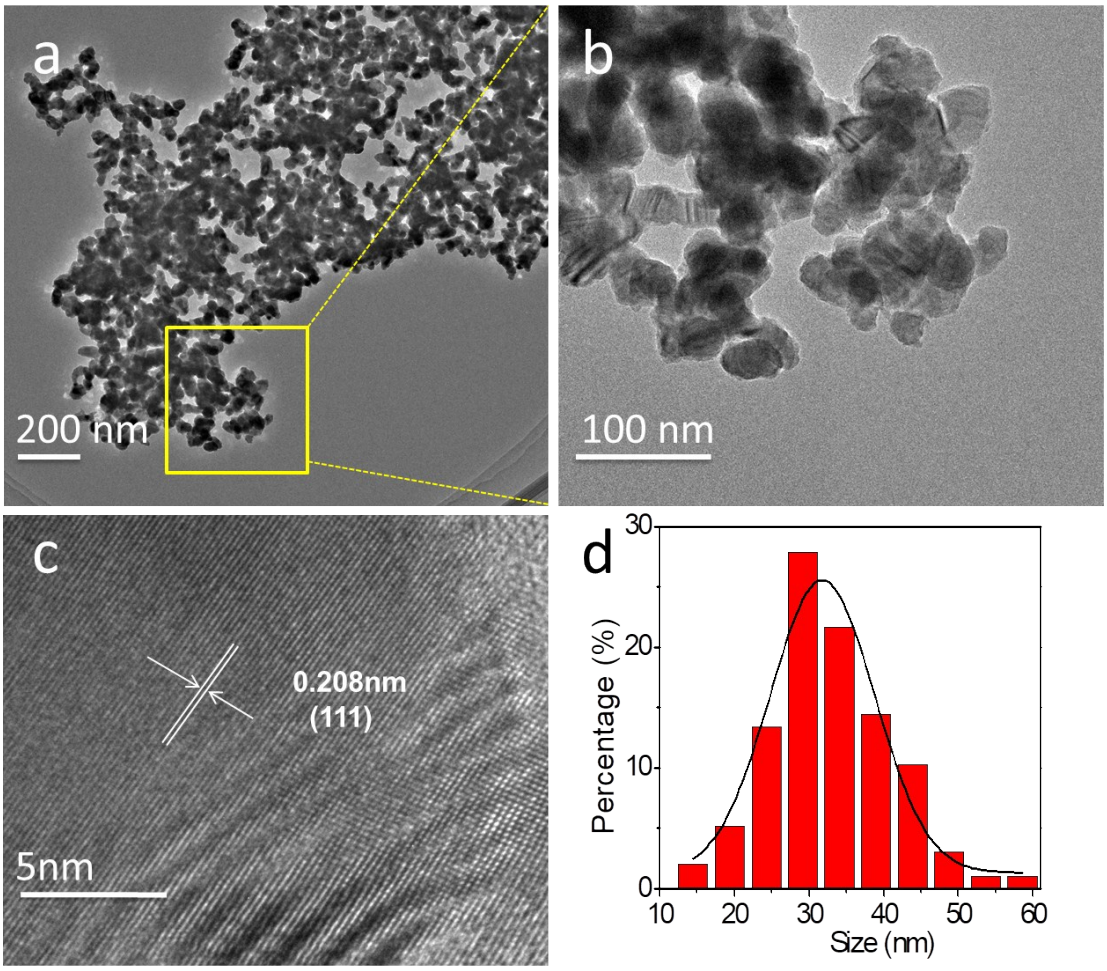

Fig. S5. (a) TEM image, (b) magnified TEM image, (c) HRTEM and (d) size distribution of Cu NPs.

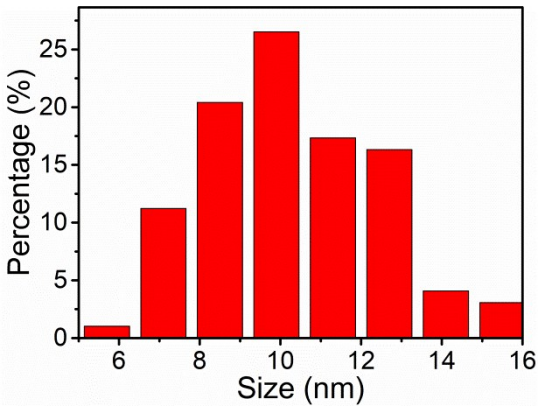

Fig. S6. Size distribution of Cu NPs in Cu/$Co(OH)_2$.

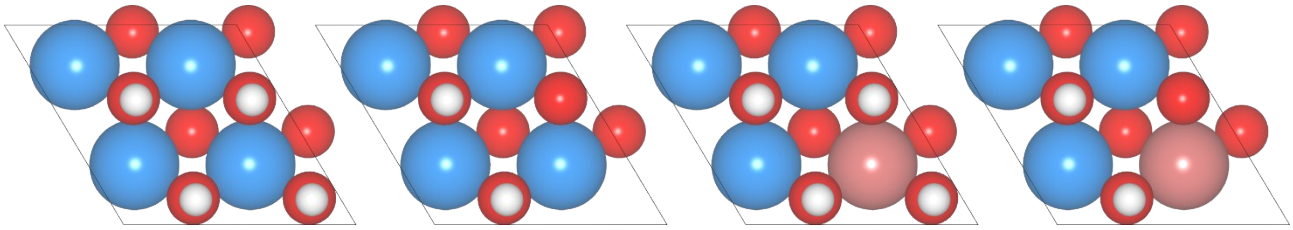

Fig. S7. Schematic surface structures of $Co(OH)_2$, Cu replaced $Co(OH)_2$ and their vacancies. Co, Cu, O, and H are shown in blue, brown, red, and white respectively.

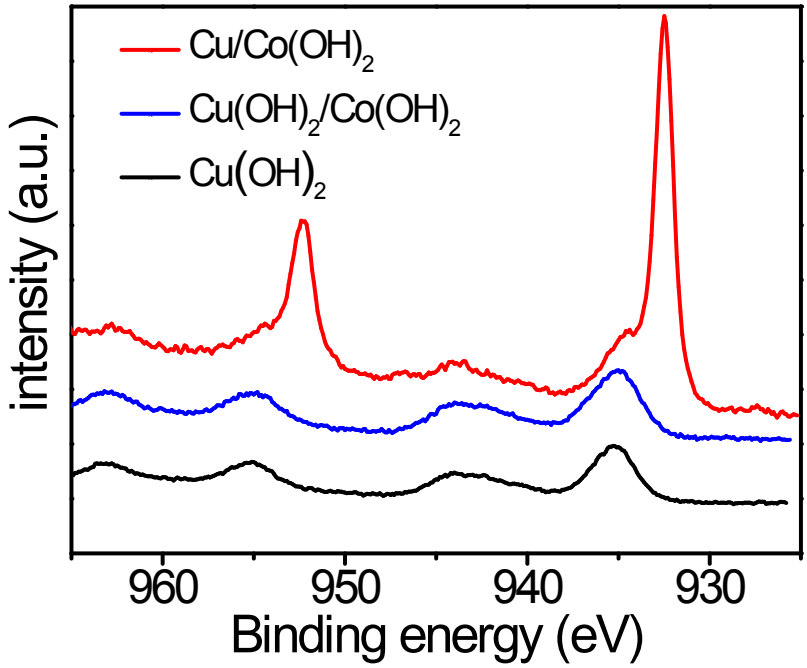

Fig. S8. Cu 2p XPS spectra of $Cu/Co(OH)_2$, $Cu(OH)_2/Co(OH)_2$ and $Cu(OH)_2$.

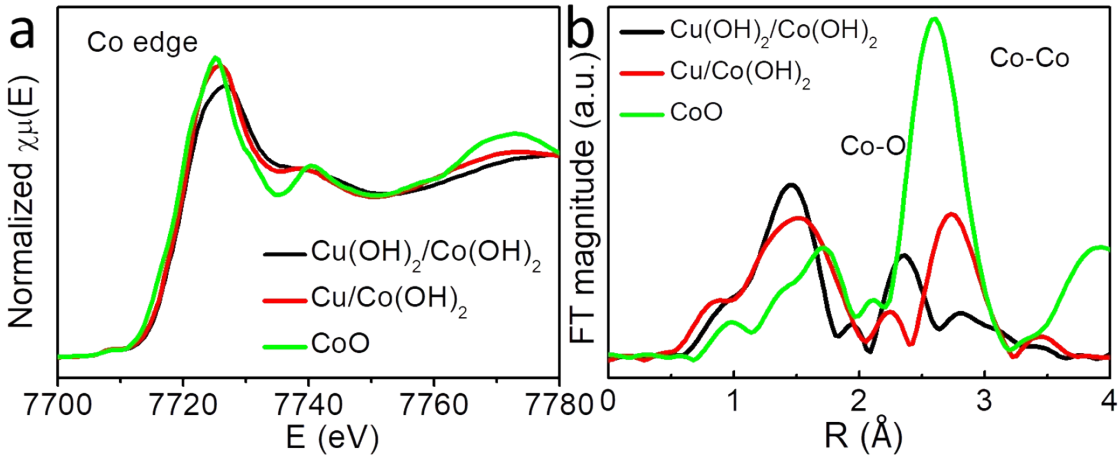

Fig. S9. (a) Co k-edge XANES and (b) Corresponding Fourier transforms spectra of $Cu(OH)_2/Co(OH)_2$, $Cu/Co(OH)_2$ and CoO.

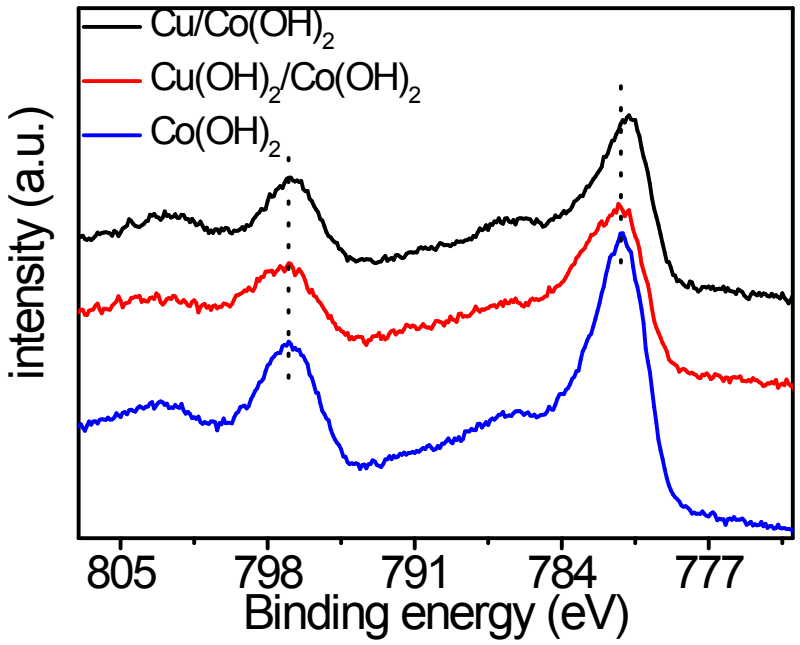

Fig. S10. Co 2p XPS spectra of $Cu/Co(OH)_2$, $Cu(OH)_2/Co(OH)_2$ and $Cu(OH)_2$.

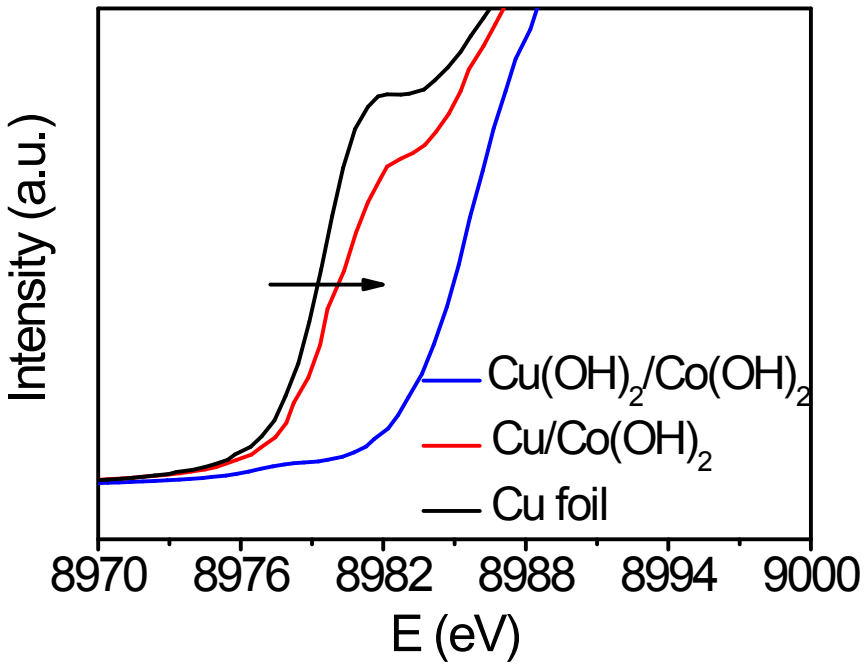

Fig. S11. Magnified XANES spectra for $Cu(OH)_2/Co(OH)_2$, $Cu/Co(OH)_2$ and Cu foil.

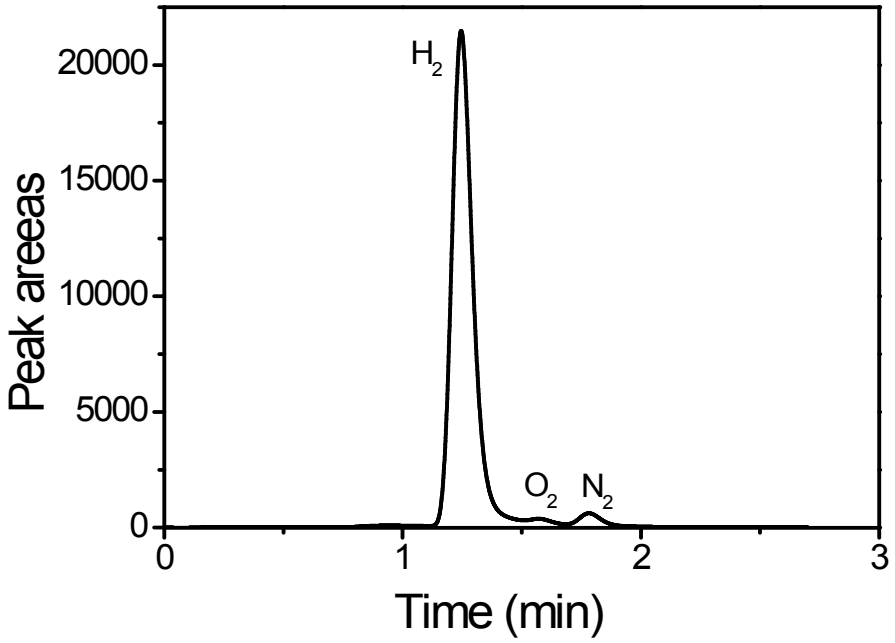

Fig. S12. Recorded peak area of gases corresponding to labeled H_2 produced in reaction systems.

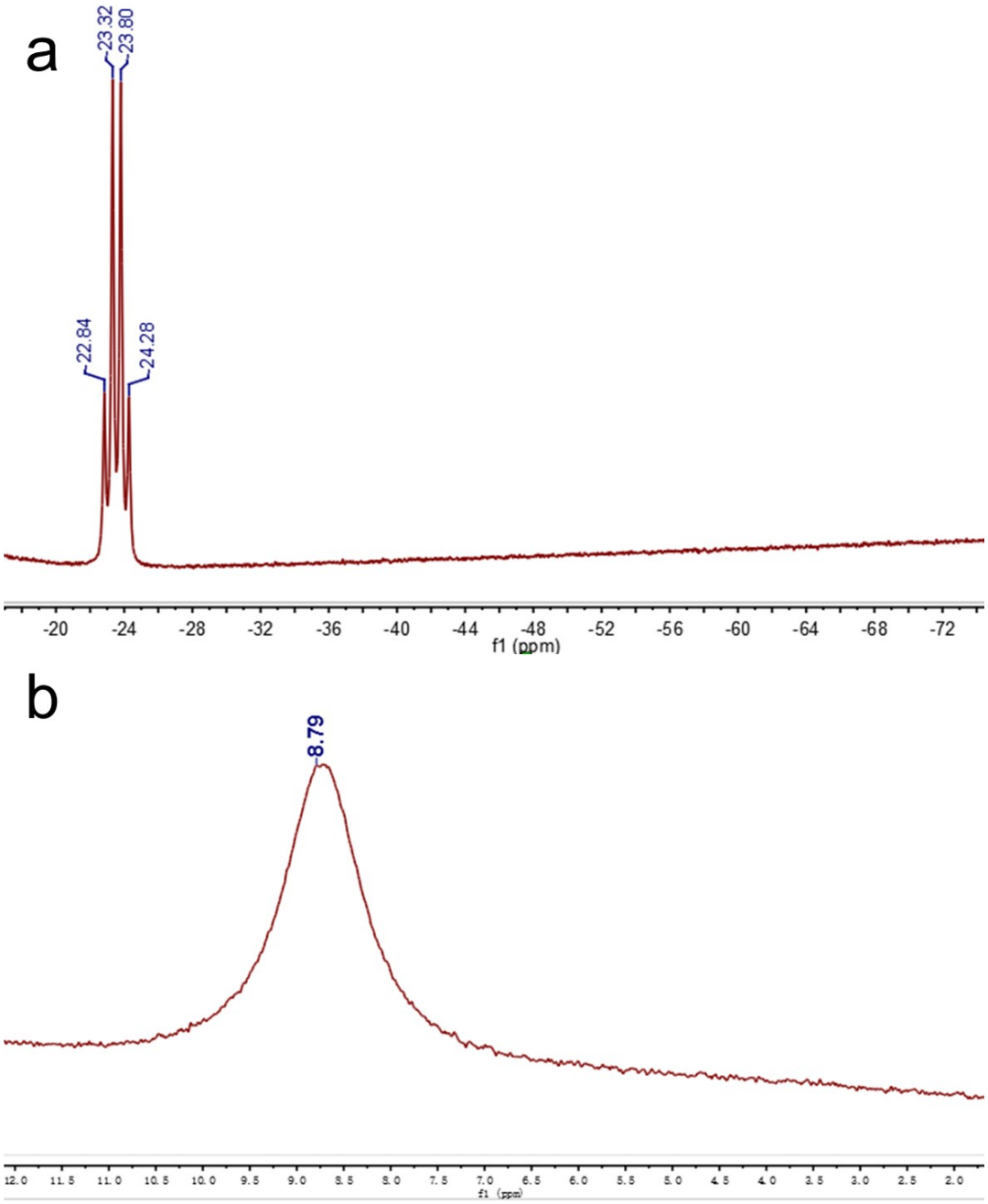

Fig. S13. ^{11}B NMR spectra of AB solution in CD_3OD (a) before reaction and (b) after reaction at 298 K.

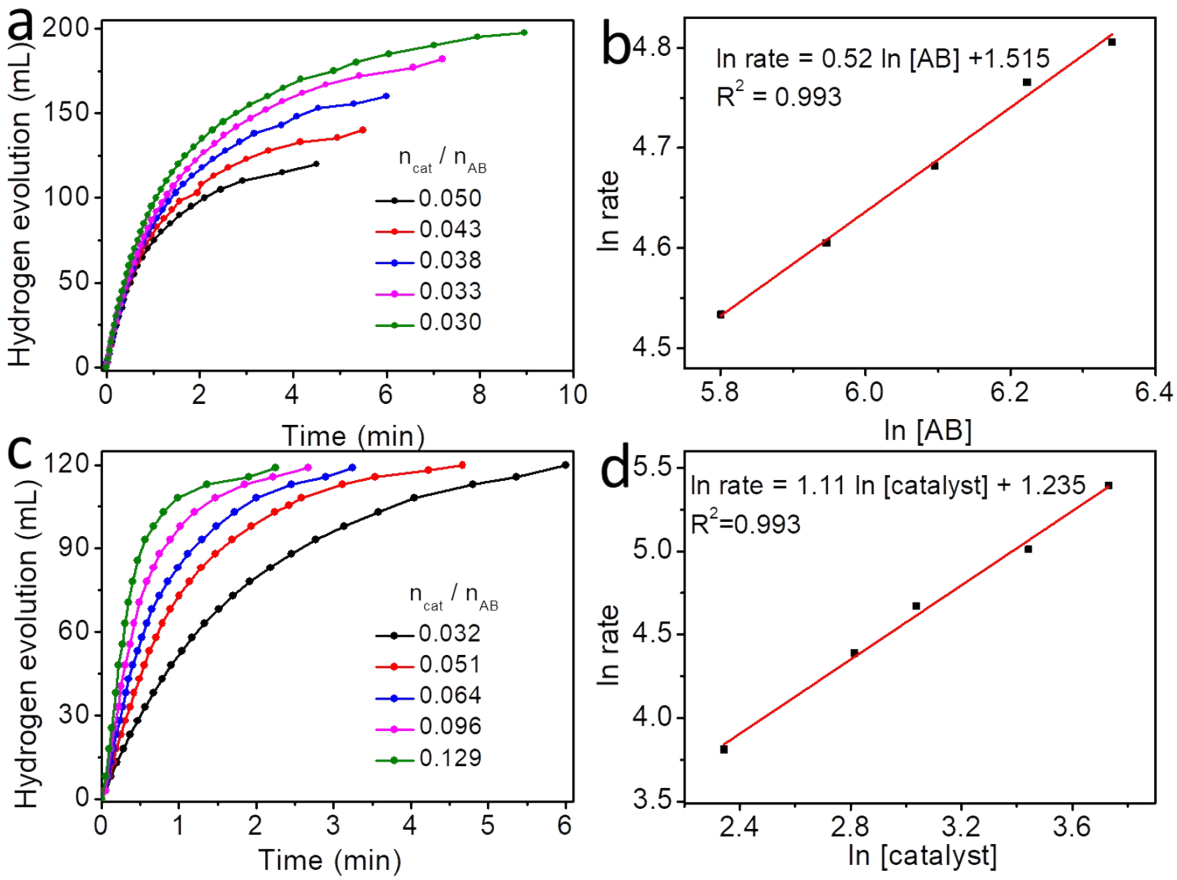

Fig. S14. Relationship between the H_2 generation rate and catalysts/AB ratios with (a) fixed amount (8 mg) of catalyst and (c) fixed amount (50 mg) of AB, respectively. Logarithmic plots of H_2 evolution rate (b) verse [AB] and (d) [catalyst] in 0.5 M NaOH methanol at 298K, respectively.

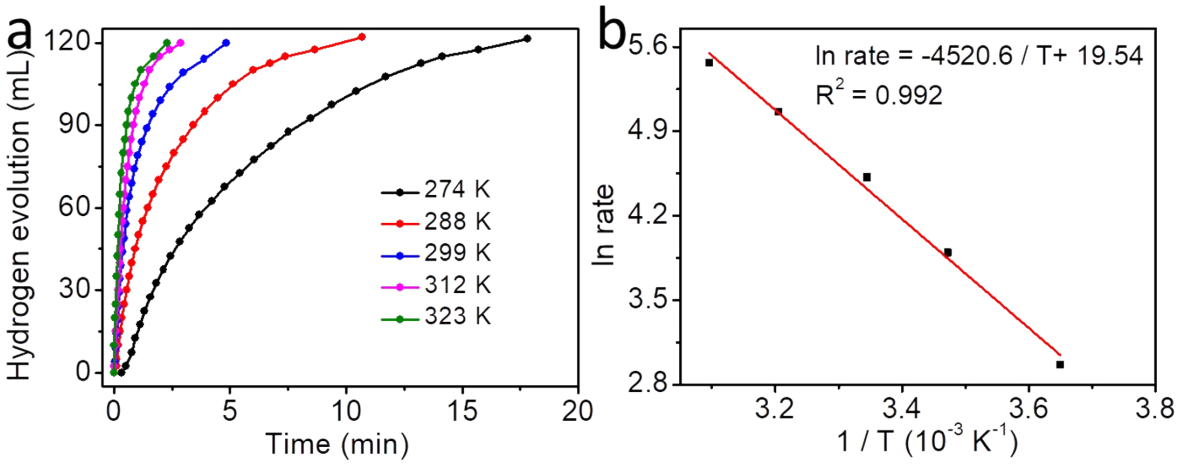

Fig. S15. (a) Relationship between the H_2 generation rate and temperature. (b) Arrhenius plot of ln rate versus 1/T.

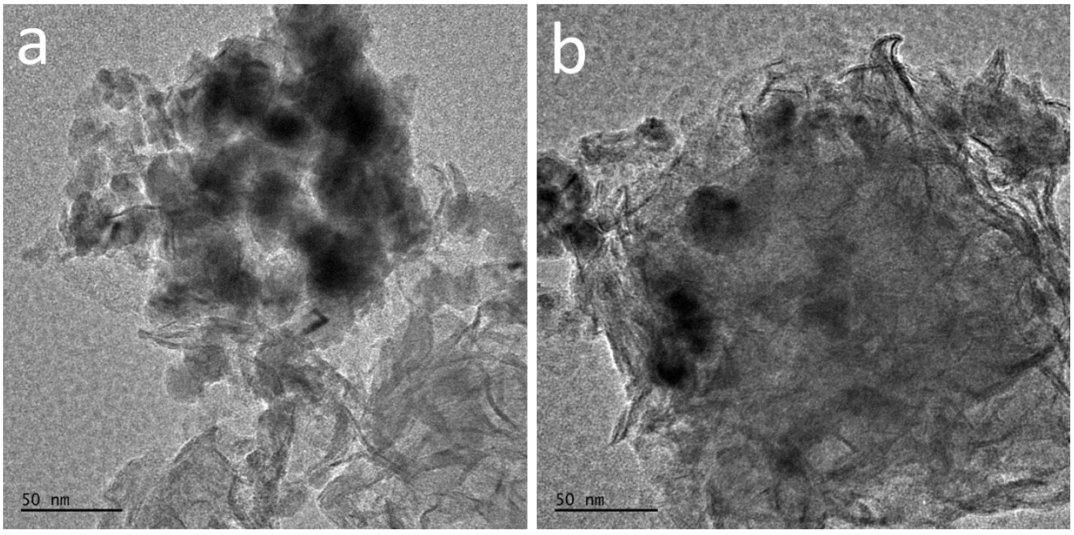

Fig. S16. TEM images of $Cu/Co(OH)_2$ after 7 runs.

Temperature dependent hydrogen evolution was measured at different temperatures ranging from 274 to 323 K to obtain the activation energy (E_a) of 37.6 kJ mol^{-1} (Fig. S13), which is smaller than some precious metal catalysts, such as Pt-based materials (86.6 kJ mol^{-1})[6] and Ru NPs (49.0 kJ mol^{-1}).[7] Long-term stability is also one key property to evaluate the catalyst, which was tested at 298 K for the $Cu/Co(OH)_2$ (Fig. 3d). After seven cycles, the activity of $Cu/Co(OH)_2$ somewhat attenuated, but was still enough to complete the full release of hydrogen within six minutes. By the analysis of size and morphology of Cu NPs after cycle experiment (Fig. S14), the decreased activity may be caused by the agglomeration of Cu NPs during experimental operation.

Table S5. Activities of catalysts in methanolysis of NH_3BH_3 reported in literatures.

	Catalyst	TOF $mol_{(H2)}\ mol_{(catalyst)}^{-1}\ min^{-1}$	Temperature (K)	Ref.
1	**$Cu/Co(OH)_2$**	**61.63**	**298**	**This work**
2	CuPd/C	53.2	298	8
3	G-$Cu_{36}Ni_{64}$	49.1	298	9
4	$Co_{48}Pd_{52}$/C	27.7	298	10
5	Cu-Cu_2O-CuO/C	24	298	11
6	PVP-stabilized Pd	22.3	298	12
7	b-CuO NA/CF	13.3	298	13
8	Co-Co_2B	7.5	298	14
9	Ni-Ni_3B	5	298	14
10	Co-Ni-B	10	298	14
11	Rh/zeolite	6.3	298	15
12	$CoCl_2$	3.7	298	16
13	$NiCl_2$	2.7	298	16
14	$PdCl_2$	1.6	298	16

References

(1) L. Maragliano and A. Fischer, *J. Chem. Phys.,* 2006, **125**, 24106.

(2) F. S. Hegner, J. R. Galán-Mascarós and N. López, *Inorg. Chem.,* 2016, **55**, 12851–12862.

(3) F. S. Hegner, D. Cardenas-Morcoso, S. Giménez, N. López and J. R. Galan-Mascaros, *ChemSusChem,* 2017, **10**, 4552–4560.

(4) F. Pertlik, *Monatsh. Chem.,* 1999, **130**, 1083–1088.

(5) M. Garcia-Ratés and N. López, *J. Chem. Theory Comput.,* 2016, **12**, 1331–1341.

(6) N. Mohajeri, A. T-Raissi and O. Adebiyi, *J. Power Sources,* 2007, **167**, 482–485.

(7) G. Chen, S. Desinan, R. Rosei, F. Rosei and D. Ma, *Chem. Eur. J.,* 2012, **18**, 7925–7930.

(8) P. Li, Z. Xiao, Z. Liu, J. Huang, Q. Li and Dao, S. *Nanotechnology,* 2015, **26**, 025401.

(9) C. Yu, J. Fu, M. Muzzio, T. Shen, D. Su, J. Zhu and S. Sun, *Chem. Mater.,* 2017, **29**, 1413–1418.

(10) D. Sun, V. Mazumder, Ö. Metin and S. Sun, *ACS Catal.,* 2012, **2**, 1290–1295.

(11) M. Yurderi, A. Bulut, İ. E. Ertas, M. Zahmakìran and M. Kaya, *Appl. Catal. B: Environ.,* 2015, **165**, 169–175.

(12) H. Erdoğan, Ö. Metin and S. Özkar, *Phys. Chem. Chem. Phys.,* 2009, **11**, 10519–10525.

(13) L. Cui, X. Cao, X. Sun, W. Wang and J. Liu, *ChemCatChem,* 2018, **10**, 710 –715.

(14) S. B. Kalidindi, A. A. Vernekar and B. R. Jagirdar, *Phys. Chem. Chem. Phys.,* 2009, **11**, 770–775.

(15) S. Çalışkan, M. Zahmakırana and S. Özkar, *Appl. Catal. B: Environ.,* 2010, **93**, 387–394.

(16) P. V. Ramachandran and P. D. Gagare, *Inorg. Chem.,* 2007, **46**, 7810–7817.